Extraction of partonic transverse momentum distributions from semi-inclusive deep inelastic scattering and Drell-Yan data

Alessandro Bacchetta,[1,2,*] Filippo Delcarro,[1,2,†] Cristian Pisano,[1,2,*] Marco Radici,[2,‡] and Andrea Signori[3,§]

[1]*Dipartimento di Fisica, Università di Pavia, via Bassi 6, I-27100 Pavia*
[2]*INFN Sezione di Pavia, via Bassi 6, I-27100 Pavia, Italy*
[3]*Theory Center, Thomas Jefferson National Accelerator Facility,*
12000 Jefferson Avenue, Newport News, VA 23606, USA
(Dated: Wednesday 8th March, 2017, 17:46)

We present an extraction of unpolarized partonic transverse momentum distributions (TMDs) from a simultaneous fit of available data measured in semi-inclusive deep inelastic scattering and in Drell-Yan processes through the production of photon and Z bosons. To connect data at different scales, we use TMD evolution at next-to-leading logarithmic accuracy. The analysis is restricted to the low-transverse-momentum region, with no matching to fixed-order calculations at high transverse momentum. We introduce specific choices to deal with TMD evolution at low scales, of the order of 1 GeV^2. This could be considered as a first attempt at a global fit of TMDs.

PACS numbers: 13.60.Le, 13.87.Fh,14.20.Dh

Contents

[*]Electronic address: `alessandro.bacchetta@unipv.it`
[†]Electronic address: `filippo.delcarro01@ateneopv.it`
[‡]Electronic address: `marco.radici@pv.infn.it`
[§]Electronic address: `asignori@jlab.org`

I. INTRODUCTION

Parton distribution functions describe the internal structure of the nucleon in terms of its elementary constituents (quarks and gluons). They cannot be easily computed from first principles, because they require the ability to carry out Quantum Chromodynamics (QCD) calculations in a nonperturbative regime. Many experimental observables in hard scattering experiments involving hadrons are related to parton distribution functions (PDFs) and fragmentation functions (FFs), in a way that is specified by factorization theorems (see, e.g., Refs. [1, 2]). These theorems also elucidate the universality properties of PDFs and FFs (i.e., the fact that they are the same in different processes) and their evolution equations (i.e., how they get modified by the change in the hard scale of the process). Availability of measurements of different processes in different experiments makes it possible to test the reliability of factorization theorems and extract PDFs and FFs through so-called global fits. On the other side, the knowledge of PDFs and FFs allows us to make predictions for other hard hadronic processes. These general statements apply equally well to standard collinear PDFs and FFs and to transverse-momentum-dependent parton distribution functions (TMD PDFs) and fragmentation functions (TMD FFs). Collinear PDFs describe the distribution of partons integrated over all components of partonic momentum except the one collinear to the parent hadron; hence, collinear PDFs are functions only of the parton longitudinal momentum fraction x. TMD PDFs (or TMDs for short) include also the dependence on transverse momentum components $k_\perp^2$. They can be interpreted as three-dimensional generalizations of collinear PDFs. Similar arguments apply to collinear FFs and TMD FFs [3].

There are several differences between collinear and TMD distributions. From the formal point of view, factorization theorems for the two types of functions are qualitatively different, implying also different universality properties and evolution equations [4]. From the experimental point of view, observables related to TMDs require the measurement of some transverse momentum component much smaller than the hard scale of the process [5, 6]. For instance, Deep-Inelastic Scattering (DIS) is characterized by a hard scale represented by the 4-momentum squared of the virtual photon ($-Q^2$). In inclusive DIS this is the only scale of the process, and access is limited to collinear PDFs and FFs. In semi-inclusive DIS (SIDIS) also the transverse momentum of the outgoing hadron (P_{hT}) can be measured [7, 8]. If $P_{hT}^2 \ll Q^2$, TMD factorization can be applied and the process is sensitive to TMDs [2].

If polarization is taken into account, several TMDs can be introduced [7, 9–12]. Attempts to extract some of them have already been presented in the past [13? –20]. In this work, we focus on the simplest ones, i.e., the unpolarized TMD PDF $f_1^q(x, k_\perp^2)$ and the unpolarized TMD FF $D_1^{q \to h}(z, P_{hT}^2)$, where z is the fractional energy carried by the detected hadron h. Despite their simplicity, the phenomenology of these unpolarized TMDs present several challenges [21]: the functional form of TMDs at low partonic transverse momentum, its possible dependence on the parton flavor [22], the implementation of TMD evolution [4, 23], the matching to fixed-order calculations in collinear factorization [24].

We take into consideration three kinds of processes: semi-inclusive DIS, and Drell–Yan processes (DY) with the production of virtual photons and Z bosons. To date, they represent almost [AB:why almost? what else could be used? AS: e^+e^- data.] all possible processes where experimental information is available for unpolarized TMD extractions. The only important process currently missing is electron-positron annihilation, which is particularly important for the determination of TMD FFs [23]. This work can therefore be considered as the first attempt at a global fit of TMDs.

The paper is organized as follows. In Sec. II, the general formalism for TMDs in SIDIS and DY processes is briefly outlined, including a description of the assumptions and approximations in the phenomenological implementation of TMD evolution equations. In Sec. III, the criteria for selecting the data analyzed in the fit are summarized and commented. In Sec. IV, the results of our global fit are presented and discussed. In Sec. V, we summarize the results and present an outlook for future analyses.

II. FORMALISM

AS: Shall we add pictures for the kinematics of SIDIS and DY data ? E.g. see Fig. 1 in [22].

A. Semi-inclusive DIS

In one-particle SIDIS, a lepton ℓ with momentum l scatters off a hadron target N with mass M and momentum P. In the final state, the scattered lepton momentum l' is measured together with one hadron h with mass M_h and momentum P_h. The corresponding reaction formula is

$$\ell(l) + N(P) \to \ell(l') + h(P_h) + X \,. \tag{1}$$

The space-like momentum transfer is $q = l - l'$, with $Q^2 = -q^2$. We introduce the usual invariants

$$x = \frac{Q^2}{2\,P\cdot q}, \qquad\qquad y = \frac{P\cdot q}{P\cdot l}, \qquad\qquad z = \frac{P\cdot P_h}{P\cdot q}, \qquad\qquad \gamma = \frac{2Mx}{Q}. \tag{2}$$

The available data refer to SIDIS hadron multiplicities, namely to the differential number of hadrons produced per corresponding inclusive DIS event. In terms of cross sections, we define the multiplicities as

$$m_N^h(x, z, |\boldsymbol{P}_{hT}|, Q^2) = \frac{d\sigma_N^h/(dx\,dz\,d|\boldsymbol{P}_{hT}|\,dQ^2)}{d\sigma_{\mathrm{DIS}}/(dx\,dQ^2)}, \tag{3}$$

where $d\sigma_N^h$ is the differential cross section for the SIDIS process and $d\sigma_{\mathrm{DIS}}$ is the corresponding inclusive one, and where $\boldsymbol{P}_{hT}$ is the component of $\boldsymbol{P}_h$ transverse to $\boldsymbol{q}$. In the single-photon-exchange approximation, the multiplicities can be written as ratios of structure functions (see [8] for details):

$$m_N^h(x, z, |\boldsymbol{P}_{hT}|, Q^2) = \frac{2\pi\,|\boldsymbol{P}_{hT}|F_{UU,T}(x, z, \boldsymbol{P}_{hT}^2, Q^2) + 2\pi\varepsilon|\boldsymbol{P}_{hT}|F_{UU,L}(x, z, \boldsymbol{P}_{hT}^2, Q^2)}{F_T(x, Q^2) + \varepsilon F_L(x, Q^2)}, \tag{4}$$

where

$$\varepsilon = \frac{1 - y - \frac{1}{4}\gamma^2 y^2}{1 - y + \frac{1}{2}y^2 + \frac{1}{4}\gamma^2 y^2}, \tag{5}$$

and the structure function $F_{XY,Z}$ corresponds to a lepton with polarization X scattering on a target with polarization Y by exchanging a virtual photon in a polarization state Z.

The semi-inclusive cross section can be expressed in a factorized form in terms of TMDs only in the kinematical limits $M^2 \ll Q^2$ and $\boldsymbol{P}_T^2 \ll Q^2$. In these limits, the structure function $F_{UU,L}$ of Eq. (4) can be neglected [25]. The structure function F_L in the denominator contains contributions involving powers of the strong coupling constant α_S at an order that goes beyond the level reached in this analysis; hence, it will be consistently neglected (see also Ref. [22]).

To express the structure functions in terms of TMD PDFs and FFs, we rely on the factorized formula for SIDIS [2, 26–33]:

$$F_{UU,T}(x, z, \boldsymbol{P}_{hT}^2, Q^2) = \sum_a \mathcal{H}_{UU,T}^a(Q^2; \mu^2) \tag{6}$$
$$\times \int d\boldsymbol{k}_\perp\, d\boldsymbol{P}_\perp\, f_1^a(x, \boldsymbol{k}_\perp^2; \mu^2)\, D_1^{a\to h}(z, \boldsymbol{P}_\perp^2; \mu^2)\, \delta(z\boldsymbol{k}_\perp - \boldsymbol{P}_{hT} + \boldsymbol{P}_\perp)$$
$$+ Y_{UU,T}(Q^2, \boldsymbol{P}_{hT}^2) + \mathcal{O}(M^2/Q^2).$$

Here, $\mathcal{H}_{UU,T}$ is the hard scattering part; $f_1^a(x, \boldsymbol{k}_\perp^2; \mu^2)$ is the TMD distribution of unpolarized partons with flavor a in an unpolarized proton, carrying longitudinal momentum fraction x and transverse momentum $\boldsymbol{k}_\perp$ at the factorization scale μ^2, which in the following we choose to be equal to Q^2. The $D_1^{a\to h}(z, \boldsymbol{P}_\perp^2; \mu^2)$ is the TMD fragmentation function describing the fragmentation of an unpolarized parton with flavor a into an unpolarized hadron h carrying longitudinal momentum fraction z and transverse momentum $\boldsymbol{P}_\perp$. The term $Y_{UU,T}$ is introduced to ensure a matching to the perturbative fixed-order calculations at higher transverse momenta.

The applicability of Eq. (6) relies on the possibility of neglecting M^2/Q^2 corrections. At large Q^2 this should not pose serious problems. However, fixed-target DIS experiments typically collect a large amount of data at relatively low Q^2 values, which may lead to problems (see, e.g., recent discussions in Refs. [34?]).

Eq. (6) can be expanded in powers of α_S. In the present analysis, we will consider only the leading order terms in α_S, i.e., stop at order α_S^0. In this case $\mathcal{H}_{UU,T}(Q^2, \mu^2) \approx 1$ and $Y_{UU,T} \approx 0$. However, perturbative corrections include large logarithms $L \equiv \log(z^2 Q^2/P_{hT}^2)$, so that $\alpha_S L \approx 1$. In the present analysis, we will take into account all powers of the form $\alpha_S^n L^{2n} \approx 1$ (Leading Logarithms –LL) and $\alpha_S^n L^n \approx 1$ (Next-to-Leading Logarithms – NNL).

In these approximations (LO in $alpha_S$ and NLL), only the first term in Eq. (6) is relevant (often in the literature this has been called W term). We expect this term to provide a good description of the structure function only in the region where $P_{hT}^2/z^2 \ll Q^2$. It can happen that $Y_{UU,T}$, defined in the standard way (see, e.g., Ref. [27]), gives large contributions also in this region, but it is admissible to redefine it in order to avoid this problem [24]. We leave a detailed treatment of the matching to the high $P_{hT}^2 \approx Q^2$ region to future investigations.

To the purpose of applying TMD evolution equations, need to calculate the Fourier transform of the the part of Eq. (6) involving TMDs. The structure function thus reduces to

$$F_{UU,T}(x, z, \boldsymbol{P}_{hT}^2, Q^2) \approx \sum_a \int_0^\infty \frac{d\zeta_T}{2\pi} \zeta_T J_0\big(\zeta_T |\boldsymbol{P}_{hT}|/z\big) \tilde{f}_1^a\big(x, \zeta_T; Q^2\big) \tilde{D}_1^{a \to h}\big(z, \zeta_T; Q^2\big).$$

E' questa la formula usata nel codice, o serve dire altro? where we introduced the Fourier transforms of the TMD PDF and FF according to

$$\tilde{f}_1^a\big(x, \zeta_T; \mu^2\big) = \int_0^\infty \frac{d|\boldsymbol{k}_\perp|}{2\pi} |\boldsymbol{k}_\perp| J_0\big(\zeta_T |\boldsymbol{k}_\perp|\big) f_1^a\big(x, \boldsymbol{k}_\perp^2; \mu^2\big), \tag{7}$$

$$\tilde{D}_1^{a \to h}\big(z, \zeta_T; \mu^2\big) = \int_0^\infty \frac{d|\boldsymbol{P}_\perp|}{2\pi z^2} |\boldsymbol{P}_\perp| J_0\big(\zeta_T |\boldsymbol{P}_\perp|/z\big) D_1^{a \to h}\big(z, \boldsymbol{P}_\perp^2; \mu^2\big). \tag{8}$$

B. Drell–Yan processes

In a Drell–Yan process, two hadrons A and B with momenta P_A and P_B collide at a center-of-mass energy squared $s = (P_A + P_B)^2$ and produce a virtual photon or a Z boson plus hadrons. The boson decays into a lepton-antilepton pair. The reaction formula is

$$A(P_A) + B(P_B) \to [\gamma^*/Z + X \to]\ell^+(l) + \ell^-(l') + X. \tag{9}$$

The invariant mass of the virtual photon is $Q^2 = q^2$ with $q = l + l'$. We introduce the rapidity of the virtual photon/Z boson

$$\eta = \frac{1}{2} \log\left(\frac{q^0 + q_z}{q^0 - q_z}\right). \tag{10}$$

where the z direction is defined along the momentum of hadron A.

The cross section can be written in terms of structure functions [35, 36]. For our purposes, we need the unpolarized cross section integrated over $d\Omega$ and over the azimuthal angle of the virtual photon,

$$\frac{d\sigma}{dQ^2 \, dq_T^2 \, d\eta} = \sigma_0^{\gamma,Z}\left(F_{UU}^1 + \frac{1}{2}F_{UU}^2\right). \tag{11}$$

The elementary cross sections are

$$\sigma_0^\gamma = \frac{4\pi\alpha_{\text{em}}^2}{3Q^2 s}, \qquad \sigma_0^Z = \frac{\pi^2\alpha_{\text{em}}}{s(\sin^2\theta_W \cos^2\theta_W)} B_R(Z \to \ell^+\ell^-)\delta(Q^2 - M_Z^2), \tag{12}$$

where θ_W is Weinberg's angle, M_Z is the mass of the Z boson, and B_R is the branching ratio for the Z boson decay in two leptons. We adopted the narrow-width approximation, i.e., we neglect contributions for $Q^2 \neq M_Z^2$. We used the values $\sin^2\theta_W = 0.2313$, $M_Z = 91.18$ GeV, and $B_R(Z \to \ell^+\ell^-) = 3.366$.

[Secondo me nella prima delle eq.(10) ci vuole π^2. Infatti, partendo da Ref.[14] abbiamo

$$\frac{d\sigma}{d^4q} = \frac{\alpha^2}{sQ^2} \frac{8\pi}{3}\left[F_{UU}^1 + \frac{1}{2}F_{UU}^2\right]$$

Ora $d^4q = dq^+ dq^- dq_x dq_y$. Lo Jacobiano della trasformazione $||dQ^2 d\eta/dq^+ dq^-|| = 2$. Mentre quello per $||dq_T^2 d\theta_q/dq_x dq_y|| = 2$. Quindi

$$\frac{d\sigma}{dQ^2 d\eta dq_T^2 d\theta_q} = \frac{1}{4}\frac{d\sigma}{d^4q} = \frac{\alpha^2}{sQ^2}\frac{2\pi}{3}\left[F_{UU}^1 + \frac{1}{2}F_{UU}^2\right]$$

L'ulteriore integrazione in $d\theta_q$ fornisce un 2π, quindi

$$\frac{d\sigma}{dQ^2 d\eta dq_T^2} = \frac{\alpha^2}{sQ^2}\frac{4\pi^2}{3}\left[F_{UU}^1 + \frac{1}{2}F_{UU}^2\right]$$

Vi torna?] [AB: I started from Eq. 57 of Ref. [36] and I integrated over the solid angle. The integration over ϕ is trivial and gives a 2π. The integration over $cos\theta$ gives a factor 8/3 in front of F_{UU}^1 and a factor 4/3 in front of F_{UU}^2. The F factor in the denominator, neglecting hadron masses, is equal to $2s$ (see first line of p. 3). Finally, there is the factor 2 in the denomininator coming from the first Jacobian of Marco.]

Similarly to the SIDIS case, in the kinematical limit $q_T^2 \ll Q^2$ and neglecting the hadron masses the structure function F_{UU}^2 can be neglected.

The longitudinal momentum fractions can be written in terms of rapidity in the following way

$$x_A = \frac{Q}{\sqrt{s}} e^\eta, \qquad\qquad x_B = \frac{Q}{\sqrt{s}} e^{-\eta}. \qquad (13)$$

Some experiments use the variable x_F, which is connected to the other variables by the following relations

$$\eta = \sinh^{-1}\left(\frac{\sqrt{s}}{Q}\frac{x_F}{2}\right), \qquad x_A = \sqrt{\frac{Q^2}{s} + \frac{x_F^2}{4}} + \frac{x_F}{2}, \qquad x_B = x_A - x_F. \qquad (14)$$

The structure function F_{UU}^1 can be written as

$$F_{UU}^1(x_A, x_B, \boldsymbol{q}_T^2, Q^2) = \sum_a \mathcal{H}_{UU}^{1a}(Q^2; \mu^2) \qquad\qquad (15)$$

$$\times \int d\boldsymbol{k}_{\perp A}\, d\boldsymbol{k}_{\perp B}\, f_1^a\big(x_A, \boldsymbol{k}_{\perp A}^2; \mu^2\big)\, f_1^{\bar{a}}\big(x_B, \boldsymbol{k}_{\perp B}^2; \mu^2\big)\, \delta\big(\boldsymbol{k}_{\perp A} - \boldsymbol{q}_T + \boldsymbol{k}_{\perp B}\big)$$
$$+ Y_{UU}^1\big(Q^2, \boldsymbol{q}_T^2\big) + \mathcal{O}\big(M^2/Q^2\big)\,.$$

As in the SIDIS case, with the above kinematical limits the Y_{UU} term and corrections from higher twists of order M^2/Q^2 or higher can be neglected. In our analysis, we consider the hard coefficients only up to leading order in the couplings, i.e.,

$$\mathcal{H}_{UU,\gamma}^{1a}(Q^2; \mu^2) \approx \frac{e_a^2}{N_c}, \qquad\qquad \mathcal{H}_{UU,Z}^{1a}(Q^2; \mu^2) \approx \frac{V_a^2 + A_a^2}{N_c}\,, \qquad (16)$$

where[1]

$$V_a = I_{3a} - 2e_a \sin\theta_W\,, \qquad\qquad A_a = I_{3a}\,. \qquad (17)$$

The structure function can be conveniently expressed as a Fourier transform of the right-handside of Eq. (15) as

$$F_{UU}^1(x_A, x_B, \boldsymbol{q}_T^2, Q^2) = \sum_a \mathcal{H}_{UU}^{1a} \int_0^\infty \frac{d\zeta_T}{2\pi}\, \zeta_T\, J_0\big(\zeta_T |\boldsymbol{q}_T|\big)\, \tilde{f}_1^a\big(x_A, \zeta_T; \mu^2\big)\, \tilde{f}_1^{\bar{a}}\big(x_B, \zeta_T; \mu^2\big)\,. \qquad (18)$$

Stessa osservazione che in SIDIS: è questa la formula usata nel codice, o serve dire altro?

C. TMDs and their evolution

Following the formalism of Refs. [2, 30], the unpolarized TMD distribution and fragmentation functions in configuration space for a parton flavor a at a certain scale μ^2 can be written as

$$\tilde{f}_1^a(x, \zeta_T; \mu^2) = \sum_{i=q,\bar{q},g} \big(C_{a/i} \otimes f_1^i\big)(x; \mu_b^2)\, e^{S(\mu_b^2, \mu^2)}\, e^{g_K(\zeta_T)\ln(\mu^2/Q_0^2)}\, \tilde{f}_{1\text{NP}}^a(x, \zeta_T)\,, \qquad (19)$$

$$\tilde{D}_1^{a \to h}(z, \zeta_T; \mu^2) = \sum_{i=q,\bar{q},g} \big(\hat{C}_{a/i} \otimes D_1^{i \to h}\big)(z; \mu_b^2)\, e^{S(\mu_b^2, \mu^2)}\, e^{g_K(\zeta_T)\ln(\mu^2/Q_0^2)}\, \tilde{D}_{1\text{NP}}^{a \to h}(z, \zeta_T)\,. \qquad (20)$$

---

[1] We remind the reader that the value of weak isospin I_3 is equal to $+1$ for u, c, t and -1 for d, s, b.

The C and $\hat{C}$ are perturbatively calculable Wilson coefficients for the TMD distribution and fragmentation functions, respectively. They are convoluted with the corresponding collinear functions according to

$$(C_{a/i} \otimes f_1^i)(x, \bar{b}_*; \mu_b^2) = \int_x^1 \frac{du}{u} \, C_{a/i}\left(\frac{x}{u}, \alpha_S(\mu_b^2)\right) \, f_1^i(u; \mu_b^2) \,, \qquad (21)$$

$$(\hat{C}_{a/i} \otimes D_1^{i \to h})(z, \bar{b}_*; \mu_b^2) = \int_z^1 \frac{du}{u} \, \hat{C}_{a/i}\left(\frac{z}{u}, \bar{b}_*; \mu_b^2\right) \, D_1^{i \to h}(u; \mu_b^2) \,. \qquad (22)$$

In the present analysis, we consider only the leading-order term in the α_S expansion, i.e.,

$$C_{a/i}\left(\frac{x}{u}, \alpha_S(\mu_b^2)\right) \approx \delta_{ai}\delta(1 - x/u), \qquad\qquad \hat{C}_{a/i}\left(\frac{z}{u}, \alpha_S(\mu_b^2)\right) \approx \delta_{ai}\delta(1 - z/u). \qquad (23)$$

As a consequence, the expression for the evolved TMD functions reduces to

$$\widetilde{f}_1^a(x, \zeta_T; \mu^2) = f_1^a(x; \mu_b^2) \, e^{S(\mu_b^2, \mu^2)} \, e^{g_K(\zeta_T)\ln(\mu^2/Q_0^2)} \, \widetilde{f}_{1\mathrm{NP}}^a(x, \zeta_T) \,, \qquad (24)$$

$$\widetilde{D}_1^{a \to h}(z, \zeta_T; \mu^2) = D_1^{a \to h}(z; \mu_b^2) \, e^{S(\mu_b^2, \mu^2)} \, e^{g_K(\zeta_T)\ln(\mu^2/Q_0^2)} \, \widetilde{D}_{1\mathrm{NP}}^{a \to h}(z, \zeta_T) \,. \qquad (25)$$

The Sudakov exponent S can be written as

$$S(\mu_b^2, \mu^2) = -\int_{\mu_b^2}^{\mu^2} \frac{dk_T^2}{k_T^2} \left[A\left(\alpha_s(k_T)\right)\ln\left(\frac{Q^2}{k_T^2}\right) + B\left(\alpha_s(k_T)\right) \right] \,, \qquad (26)$$

The convolutions are only valid for small $\zeta_T \ll 1/\Lambda_{\mathrm{QCD}}$. At larger ζ_T, the TMDs need to match the nonperturbative expressions $\widetilde{f}_{1\mathrm{NP}}^a$ and $\widetilde{D}_{1\mathrm{NP}}^{a \to h}$, respectively, that must be constrained by fitting experimental data. The evolution of TMDs from the initial scale Q_0 to μ is carried out through perturbatively calculable Sudakov factors S and $\hat{S}$, respectively, and through a nonperturbative universal term g_K at large ζ_T that accounts for the radiation of soft gluons emitted by the considered parton.

The matching between small (perturbative) and large (nonperturbative) ζ_T is controlled by the μ_b scale, which naturally should be proportional to $1/\zeta_T$. We choose

$$\mu_b = \frac{2e^{-\gamma_E}}{\bar{b}_*} \,, \qquad (27)$$

where γ_E is the Euler constant and

$$\bar{b}_* \equiv b_{\max}\left(\frac{1 - e^{-\zeta_T^4/b_{\max}^4}}{1 - e^{-\zeta_T^4/b_{\min}^4}}\right)^{1/4} \,. \qquad (28)$$

This variable replaces the simple dependence upon ζ_T in the convolutions of Eqs. (21), (22) and in the perturbative Sudakov factors S and $\hat{S}$; namely, in the perturbative parts of the TMD definitions of Eqs. (24), (25). In fact, at large ζ_T these parts are no longer reliable. Therefore, the $\bar{b}_*$ is chosen to saturate on the maximum value $b_{\max}$, as suggested by the CSS formalism [2, 30].[2] On the other hand, at small ζ_T the TMD formalism is not reliable and should be matched to the fixed-order collinear calculations. The way the matching is implemented is arbitrary. In any case, the TMD contribution can be arbitrarily modified at small ζ_T. In our approach, we choose to saturate $\bar{b}_*$ at the minimum value $b_{\min} \propto 1/Q$. With the appropriate choices, for $\zeta_T = 0$ the Sudakov exponent vanishes, as it should [38 ?]. Our choice partially corresponds to modifying the resummed logarithms as in Ref. [39] and to other similar modifications proposed in the literature [24 ?]. One advantage of these kind of prescriptions is that by integrating over the impact parameter ζ_T, the collinear expression for the cross section, in terms of collinear PDFs, is recovered, at least at leading order [24].

AB: I disagree with the following statement In general, both $b_{\max}$ and $b_{\min}$ must not be considered as free parameters; rather, they should be regarded as arbitrary scales separating perturbative from nonperturbative regimes [40]. We choose to fix them to the values

$$b_{\max} = 2e^{-\gamma_E} \text{ GeV}^{-1} = 1.123 \text{ GeV}^{-1}, \qquad\qquad b_{\min} = 2e^{-\gamma_E}/Q \,. \qquad (29)$$

The motivations are the following:

---

[2] We remind that different schemes are possible to deal with the high-ζ_T region like the so-called "complex-b prescription" [37].

- with the above choices, the scale μ_b is constrained between 1 GeV and Q, so that the collinear PDFs are never computed at a scale lower than 1 GeV and the lower limit of the integrals contained in the definition of the perturbative Sudakov factor can never become larger than the upper limit;

- at $Q_0 = 1$ GeV, $b_{\max} = b_{\min}$ and there are no evolution effects; the TMD is simply given by the corresponding collinear function multiplied by a nonperturbative contribution depending on $k_\perp$ (plus possible corrections of order α_S from the Wilson coefficients) .

Following Refs. [41–43], for the nonperturbative Sudakov factor we make the traditional choice $g_K(\zeta_T) = -g_2 \zeta_T^2/2$ with g_2 a free parameter. Recently, several alternative forms have been proposed [40, 44] including the suggestion of not including such term [45].

We parametrize the intrinsic nonperturbative parts of the TMDs in the following ways

$$\widetilde{f}_{1\mathrm{NP}}^a(x, \zeta_T) = e^{-\langle \boldsymbol{k}_{\perp a}^2 \rangle \frac{\zeta_T^2}{4}} \left(1 - \frac{\lambda \langle \boldsymbol{k}_{\perp a}^2 \rangle^2}{1 + \lambda \langle \boldsymbol{k}_{\perp a}^2 \rangle} \frac{\zeta_T^2}{4} \right) , \tag{30}$$

$$\widetilde{D}_{1\mathrm{NP}}^{a \to h}(z, \zeta_T) = \frac{\langle \boldsymbol{P}_{\perp a \to h}^2 \rangle \, e^{-\langle \boldsymbol{P}_{\perp a \to h}^2 \rangle \frac{\zeta_T^2}{4}} + \lambda_F \, \langle \boldsymbol{P}_{\perp a \to h}'^2 \rangle \left(1 - \langle \boldsymbol{P}_{\perp a \to h}'^2 \rangle \frac{\zeta_T^2}{4} \right) \, e^{-\langle \boldsymbol{P}_{\perp a \to h}'^2 \rangle \frac{\zeta_T^2}{4}}}{\langle \boldsymbol{P}_{\perp a \to h}^2 \rangle + \lambda_F \, \langle \boldsymbol{P}_{\perp a \to h}'^2 \rangle} . \tag{31}$$

After performing the anti-Fourier transform, the $f_{1\mathrm{NP}}$ and $D_{1\mathrm{NP}}$ in momentum space correspond to the normalized linear combination of a Gaussian and a weighted Gaussian:

$$f_{1\mathrm{NP}}^a(x, \boldsymbol{k}_\perp) = \frac{1}{\pi} \frac{\left(1 + \lambda \boldsymbol{k}_\perp^2 \right)}{\langle \boldsymbol{k}_{\perp a}^2 \rangle + \lambda \, \langle \boldsymbol{k}_{\perp a}^2 \rangle^2} \, e^{-\frac{\boldsymbol{k}_\perp^2}{\langle \boldsymbol{k}_{\perp a}^2 \rangle}} , \tag{32}$$

$$D_{1\mathrm{NP}}^{a \to h}(z, \boldsymbol{P}_\perp) = \frac{1}{\pi} \frac{1}{\langle \boldsymbol{P}_{\perp a \to h}^2 \rangle + \lambda_F \, \langle \boldsymbol{P}_{\perp a \to h}'^2 \rangle^2} \left(e^{-\frac{\boldsymbol{P}_\perp^2}{\langle \boldsymbol{P}_{\perp a \to h}^2 \rangle}} + \lambda_F \, \boldsymbol{P}_\perp^2 \, e^{-\frac{\boldsymbol{P}_\perp^2}{\langle \boldsymbol{P}_{\perp a \to h}'^2 \rangle}} \right) . \tag{33}$$

Based on the analyses of Refs. [22, 23], we consider that the Gaussian width of the TMD distribution depends on the parton flavor a and on its fractional momentum x according to

$$\langle \boldsymbol{k}_{\perp a}^2 \rangle(x) = \langle \hat{\boldsymbol{k}}_{\perp a}^2 \rangle \frac{(1-x)^\alpha \, x^\sigma}{(1-\hat{x})^\alpha \, \hat{x}^\sigma} , \tag{34}$$

where α, σ, and $\langle \hat{\boldsymbol{k}}_{\perp a}^2 \rangle \equiv \langle \boldsymbol{k}_{\perp a}^2 \rangle(\hat{x})$ with $\hat{x} = 0.1$, are free parameters. Similarly, we have

$$\langle \boldsymbol{P}_{\perp a \to h}^2 \rangle(z) = \langle \hat{\boldsymbol{P}}_{\perp a \to h}^2 \rangle \frac{(z^\beta + \delta) \, (1-z)^\gamma}{(\hat{z}^\beta + \delta) \, (1-\hat{z})^\gamma} , \tag{35}$$

where β, γ, δ, and $\langle \hat{\boldsymbol{P}}_{\perp a \to h}^2 \rangle \equiv \langle \boldsymbol{P}_{\perp a \to h}^2 \rangle(\hat{z})$ with $\hat{z} = 0.5$, are free parameters. Mention that also the other variance in the TMD FF has the same kinematic dependence.

III.   DATA ANALYSIS

One of the main goals of our fit is to test the universality of TMD parton distribution and fragmentation functions among different processes. To achieve this we included measurements taken from SIDIS, Drell-Yan and Z boson production from different experimental collaborations. In this chapter we describe the data sets considered for each process and the reasons behind the kinematic cuts applied.

Tab. I refers to the data sets for SIDIS off proton target (HERMES experiment) and presents their kinematic ranges. The same holds for Tab. II, Tab. III, Tab. IV for SIDIS off deuteron (HERMES and COMPASS experiments), Drell-Yan events at low energy and Z boson production respectively. For each kinematic variable in all the considered data sets, we fit the average value in each bin.

AS: specify how we treat the nuclear targets, like D= p+n incoherent, then DY ... .

A.   Hermes data

The semi-inclusive DIS data are taken from HERMES [46] and COMPASS [47] experiments. Both HERMES and COMPASS data have been already analyzed in a previous works, e.g. [22, 48].

HERMES data [46] are grouped in two sets, distinguished by the inclusion or subtraction of the vector meson contribution. In our work we considered only the data set where contributions from vector mesons have been subtracted. The collaboration measured the multiplicities for SIDIS in a fixed-target experiment using hydrogen (p) and deuteron (D) targets and separating charged pions and kaons produced in the final state. The data include 8 different channels for every combination of target and final-state hadron for a total of 2688 points.

These are grouped in bins of (x, z, Q^2, P_{hT}) with the average values of (x, Q^2) ranging from about $(0.04, 1.25 \text{ GeV}^2)$ to $(0.4, 9.2 \text{ GeV}^2)$. The collinear energy fraction z in (2) ranges in $0.1 \leq z \leq 0.9$. The transverse momentum of the detected hadron satisfies $0.1 \text{ GeV} \leq |P_{hT}| \leq 1 \text{ GeV}$.

B.   Compass data

Compass collaboration extracted multiplicities of charge-separated but unidentified hadrons produced in SIDIS off a deuteron (^{6}LiD) target [47]. The data are organised in multidiensional bins of (x, z, Q^2, P_{hT}). The number of data is an order of magnitude higher compared to the HERMES experiment.

The data cover a range in (x, Q^2) from $(0.0052, 1.11 \text{ GeV}^2)$ to $(0.0932, 7.57 \text{ GeV}^2)$ and the interval $0.2 \leq z \leq 0.8$. Similarly to HERMES , for COMPASS $P_{hT}^2 \lesssim 1 \text{ GeV}^2$.

To avoid issues related to the normalization of COMPASS multiplicities (see the *erratum* to [47]), we normalize all the data in (x, z, Q^2) to the value of the first bin in P_{hT}^2. We define the *normalized* multiplicity as:

$$m_{\text{norm}}(x, z, \boldsymbol{P}_{hT}^2, Q^2) = \frac{m_N^h(x, z, \boldsymbol{P}_{hT}^2, Q^2)}{m_N^h(x, z, \min[\boldsymbol{P}_{hT}^2], Q^2)} \ , \tag{36}$$

where the multiplicity m_N^h is defined in (3). Fitting normalized multiplicities the first data point of each bin is considered as a fixed parameter and excluded from the degrees of freedom of the system.

The application of the TMD formalism to SIDIS crucially depends on the capability of identifying the current fragmentation region. This task has been recently discussed in [34], where the authors point out a possible overlap among different fragmentation regions when the hard scale Q is sufficiently low. In this paper we do not tackle this problem and we leave it to future studies. As described in Tabs. I and II, we identify the current fragmentation region operating a cut on z only, namely $0.2 < z < 0.7$.[3]

Another requirement for the applicability of TMD factorization is the presence of two separate hard scales in the process. In SIDIS, those are the Q^2 and P_{hT}^2, which should satisfy the hierarchy $\Lambda_{\text{QCD}}^2 \ll P_{hT}^2 \ll Q^2$. In order to satisfy $\Lambda_{\text{QCD}}^2 \ll Q^2$, we request $Q^2 > 1.4 \text{ GeV}^2$. The second condition is $P_{hT}^2 \ll Q^2$, together with the further constraint $P_{hT}^2 / z^2 \ll Q^2$. In our analysis we relax [4] these conditions and implement them as $P_{hT} < \min[0.2 \, Q, 0.7 \, Qz] + 0.5$

---

[3] The implementation of the "collinearity" criterion proposed in [34] crucially depends on the value of $\langle k_T^2 \rangle$, features that requires independent determinations of the partonic properties.

[4] AS [comment to ourselves]: adding 0.5 GeV might be a bit "extreme", since we could probe the $P_{hT} > Q$ region where a matching to fixed-order calculations should be taken into account.

GeV. The specific values of the terms are chosen to maximize the goodness of the fit procedure and not to exclude too many data points All these choices are summarized in Tabs. I and II.

C. Low-energy Drell-Yan data

We analyze Drell-Yan events collected by fixed-target experimets at low-energy. These data set have been considered also in previous works, e.g. [49]. We use data from E288 [50] measured at $\sqrt{s} = 19.4$, 23.8 and 27.4 GeV^2, denoted with the label "200", "300" and "400" respectively. AS: why these numbers? We also include data from E605 [51] at $\sqrt{s} = 38.8$ GeV^2.

The explored Q values are higher compared to the SIDIS case, see Tab. III. E288 provides data at fixed rapidity, whereas E605 explores a range of values for x_F (see (14)). As discussed for SIDIS data, we can apply TMD factorization if $\Lambda_{QCD}^2 \ll q_T^2 \ll Q^2$, where q_T is the transverse momentum of the intermediate electroweak boson, reconstructed from the kinematics of the final state leptons. As done for SIDIS, we choose $q_T < 0.2\,Q + 0.5$ GeV. Again, the values of the coefficients are chosen to maximize the goodness of the fit and to not exclude too many points.

D. Z-boson production data

In order to reach higher Q and q_T values, we also consider Z boson production in collider experiments at Tevatron. We analyze data from CDF and D0, collected during Tevatron Run I [52, 53] at $\sqrt{s} = 1.8$ TeV and Run II [54, 55] at $\sqrt{s} = 1.96$ TeV. The invariant mass distribution peaks at the Z-pole, $Q = M_Z$, while the transverse momentum of the exchanged Z ranges in $0 < q_T < 20$ GeV. We use the same kinematic condition applied to Drell-yan events: $q_T < 0.2\,Q + 0.5$ GeV $= 18.7$ GeV, since Q is fixed to M_Z.

The observable is $d\sigma/dq_T$, apart from the case of D0 Run II, for which the published data refer to $1/\sigma \times d\sigma/dq_T$. In order to work with the same observable in all the cases considered, we multiply the D0-Run II data by the total cross section of the process $\sigma_{exp} = 255.8 \pm 16$ pb [55]. in this case, we add in quadrature the uncertainties of the total cross section and of the published data.

We normalize our functional form with factors listed in Tab. IV. These are the same normalization factors used in [49] to fit Z boson production and differ from the experimental ones.

	HERMES $p \to \pi^+$	HERMES $p \to \pi^-$	HERMES $p \to K^+$	HERMES $p \to K^-$
Reference	[46]			
Cuts	$Q^2 > 1.4$ GeV^2			
	$0.2 < z < 0.7$			
	$P_{hT} < \text{Min}[0.2\,Q, 0.7\,Qz] + 0.5$ GeV			
Points	190	190	189	187
Max. Q^2	9.2 GeV^2			
x range	$0.06 < x < 0.4$			

TABLE I: Semi-inclusive DIS proton-target data (Hermes experiment).

E. The replica method

AS: I edited a bit the text, but some overlap remains in this section with the text in [22].

In this section we describe the replica method and we give a definition of the χ^2 function minimized by the fit procedure. The fit and the error analysis were carried out using a similar Monte Carlo approach as in Ref. [22, 56, 57] and taking inspiration from the work of the Neural-Network PDF (NNPDF) collaboration (see, e.g., [58–60]). The approach consists in creating $\mathcal{M}$ replicas of the data points. In each replica (denoted by the index r), each data point i is shifted by a Gaussian noise with the same variance as the measurement. Each replica, therefore, represents a possible outcome of an independent experimental measurement, which we denote by $m_{N,r}^h(x, z, \boldsymbol{P}_{hT}^2, Q^2)$. The number

	HERMES $D \to \pi^+$	HERMES $D \to \pi^-$	HERMES $D \to K^+$	HERMES $D \to K^-$	COMPASS $D \to h^+$	COMPASS $D \to h^-$
Reference	[46]				[47]	
Cuts	$Q^2 > 1.4$ GeV^2 $0.2 < z < 0.7$ $P_{hT} < \mathrm{Min}[0.2\,Q, 0.7\,Qz] + 0.5$ GeV					
Points	190	190	189	189	3125	3127
Max. Q^2	9.2 GeV^2				10 GeV^2	
x range	$0.06 < x < 0.4$				$0.006 < x < 0.12$	
Notes					Observable: $m_{\mathrm{norm}}(x, z, \boldsymbol{P}_{hT}^2, Q^2)$, eq. (36)	

TABLE II: Semi-inclusive DIS deuteron-target data (Hermes and Compass experiments).

	E288 200	E288 300	E288 400	E605
Reference	[50]	[50]	[50]	[51]
Cuts	$q_T < 0.2\,Q + 0.5$ GeV			
Points	45	45	78	35
$\sqrt{s}$	19.4 GeV	23.8 GeV	27.4 GeV	38.8 GeV
Q range	4-9 GeV	4-9 GeV	5-9, 11-14 GeV	7-9, 10.5-18 GeV
Kin. var.	y=0.4	y=0.21	y=0.03	$-0.1 < x_F < 0.2$

TABLE III: Low energy Drell-Yan data collected by the E288 and E605 experiments at Tevatron, with different center-of-mass energies.

	CDF Run I	D0 Run I	CDF Run II	D0 Run II
Reference	[52]	[53]	[54]	[55]
Cuts	$q_T < 0.2\,Q + 0.5$ GeV = 18.7 GeV			
Points	31	14	37	8
$\sqrt{s}$	1.8 TeV	1.8 TeV	1.96 TeV	1.96 TeV
Normalization	1.114	0.992	1.049	1.048

TABLE IV: Z boson production data collected by the CDF and D0 experiments at Tevatron, with different center-of-mass energies.

of replicas is chosen so that the mean and standard deviation of the set of replicas accurately reproduces the original data points. We see that 200 replicas are sufficient for the purpose.

A minimization procedure is applied to each replica separately, by minimizing the following error function: [5]

$$
E_r^2(\{p\}) = \sum_i \frac{\left(m_{N,r}^h(x_i, z_i, \boldsymbol{P}_{hTi}^2, Q_i^2) - m_{N,\mathrm{theo}}^h(x_i, z_i, \boldsymbol{P}_{hTi}^2; \{p\})\right)^2}{\left(\Delta m_{N,\mathrm{stat}}^{h\ 2} + \Delta m_{N,\mathrm{sys}}^{h\ 2}\right)(x_i, z_i, \boldsymbol{P}_{hTi}^2, Q_i^2) + \left(\Delta m_{N,\mathrm{theo}}^h(x_i, z_i, \boldsymbol{P}_{hTi}^2)\right)^2} \ . \tag{37}
$$

The sum runs over the i experimental points, including all species of targets N and final-state hadrons h. In each z bin for each replica the values of the collinear fragmentation functions $D_1^{a \to h}$ are independently modified with a Gaussian noise with standard deviation equal to the theoretical error $\Delta D_1^{a \to h}$. In this work we rely on different parametrizations

---

[5] Note that the error for each replica is taken to be equal to the error on the original data points. This is consistent with the fact that the variance of the $\mathcal{M}$ replicas should reproduce the variance of the original data points.

for $D_1^{a \to h}$: for pions we use the DSEHS analysis [61] at NLO in α_s; for kaons we use the DSS paranetrization [62] at LO in α_s. The uncertainties $\Delta D_1^{a \to h}$ are estimated from the plots in [63]; they represents the only source of uncertainty in $\Delta m_{N,\text{theo}}^h$. Statistical and systematical experimental uncertainties $\Delta m_{N,\text{stat}}^h$ and $\Delta m_{N,\text{sys}}^h$ are taken from the experimental collaborations. We do not take into account the covariance among different kinematic bins.

MINUIT minimizes the error function in (37) calculating its gradient with respect to the vector of parameters $\{p\}$. The final outcome is a set of $\mathcal{M}$ different vectors of best-fit parameters, $\{p_{0r}\}$, $r = 1, \dots \mathcal{M}$, with which we can calculate any observable, its mean, and its standard deviation. The distribution of these values needs not to be necessarily Gaussian. In fact, in this case the 1σ confidence interval is different from the 68% interval. The latter can simply be computed for each experimental point by rejecting the largest and the lowest 16% of the $\mathcal{M}$ values.

Although the minimization is performed on the function defined in (37), the agreement of the $\mathcal{M}$ replicas with the original data is better expressed in terms of a χ^2 function defined as in (37) but with the replacement $m_{N,r}^h \to m_N^h$, i.e., with respect to the original data set. If the model is able to give a good description of the data, the distribution of the $\mathcal{M}$ values of $\chi^2/\text{d.o.f.}$ should be peaked around one.

IV. RESULTS

AS: Filippo, can you please check the final plots? I can't run the notebooks in Dropbox because of a problem with Mathematica.

In the following we detail the results of a fit to the data sets described in Sec. III with a a flavor-independent configuration for the transverse momentum dependence of unpolarized TMDs. In Tab. V we present the total χ^2. The number of degrees of freedom (d.o.f.) is given by the number of data points analyzed reduced by the number of free parameters in the error function. The overall quality of the fit is good, with a global $\chi^2/\text{d.o.f.} = 1.55 \pm 0.05$. Uncertainties are computed as the 68% confidence level (C.L.) from the replica methodology.

Points	Parameters	χ^2	$\chi^2/\text{d.o.f.}$
8059	11	12629 ± 363	1.55 ± 0.05

TABLE V: Total number of points analyzed, number of free parameters and χ^2 values.

A. Agreement between data and theory

The partition of the global χ^2 among SIDIS off proton, SIDIS off deuteron, Drell-Yan and Z production events is given in Tab. VI, VII, VIII, IX respectively.

Semi-inclusive DIS

For SIDIS at HERMES off a proton, events with a kaon in the final state have in general a lower χ^2. This is due to the large uncertainties for the kaon FFs. The major contribution to the χ^2 comes from events with a π^+ in the final state. In [22, 64] a poor agreement between experiment and theory (which relies on the DSS parametrization [62] for collinear FFs) at the level of the collinear multiplicities affected the quality of the fit, especially for $\pi^{\pm}$. Instead, in this work we use a newer parametrization of the collinear FFs (DSEHS [61]), based on a fit which includes HERMES collinear pion multiplicities. This significantly improves the agreement at the collinear level with respect to [22, 64]. The poor χ^2 for $\pi^{\pm}$ production off a proton at HERMES is mainly due to a bad agreement in the TMD multiplciities at low z values (see the first two blocks from the top in Fig. 1). For kaon production off the proton at HERMES the agreement at low z is better than for the pions (see the first two blocks from the top in Fig. 2), which, combined with larger uncertainties, results in lower χ^2.

For SIDIS at HERMES off a deuteron, the situation is slightly different with respect to the proton case. For pion production the χ^2 is lower with respect to the scattering off a proton because the experimental uncertainties for $D \to \pi^{\pm}$ are slightly larger than for $p \to \pi^{\pm}$ (compare the first two blocks from the top with the last two ones in Fig. 1). On the contrary, for kaon production the χ^2 is higher with respect to the scattering off a proton because the experimental uncertainties for $D \to K^{\pm}$ are slightly smaller than for $p \to K^{\pm}$ (compare the first two blocks from the top with the last two ones in Fig. 2).

	HERMES $p \to \pi^+$	HERMES $p \to \pi^-$	HERMES $p \to K^+$	HERMES $p \to K^-$
Points	190	190	189	187
χ^2/points	4.83	2.47	0.91	0.82

TABLE VI: Number of points analyzed and χ^2 values for SIDIS off a proton target.

Fixing the target and comparing pion and kaon production at HERMES , we see that the χ^2 for kaons is in general lower than for pions. This is because the theoretical uncertainty for $D_1^{a \to K}$ is larger than the one for $D_1^{a \to \pi}$ [22, 63], even if the experimental uncertainties are in general smaller for kaons.

SIDIS at COMPASS involves scattering off deuteron only, $D \to h^{\pm}$, and we identify $h \equiv \pi$. The quality of the agreement between theory and COMPASS data is better than in the case of pion production at HERMES . This depends on at least two factors. First: the fit is essentially driven by the COMPASS data, since the number of points in COMPASS is much higher than in HERMES . Moreover, the observable that we fit for the case of COMPASS is the normalized multiplicity, defined in (36). This automatically eliminates any possible tension between theory and data due to normalization effects.

	HERMES $D \to \pi^+$	HERMES $D \to \pi^-$	HERMES $D \to K^+$	HERMES $D \to K^-$	COMPASS $D \to h^+$	COMPASS $D \to h^-$
Points	190	190	189	189	3125	3127
χ^2/points	3.46	2.00	1.31	2.54	1.11	1.61

TABLE VII: Number of points analyzed and χ^2 values for SIDIS off a deuteron target.

Fig. 1 presents the agreement between the theoretical formula in (3) and the HERMES multiplicities for production of pions off a proton and a deuteron. Different $\langle x \rangle$, $\langle z \rangle$ and $\langle Q^2 \rangle$ bins are displayed as a funciton of the transverse momentum of the dected hadron P_{hT}. The grey bands are an envelope of the 200 replica of best-fit curves. For every point in P_{hT} we apply a 68% C.L. selection criterion. Points marked with different symbols and colors correspond to different $\langle z \rangle$ values. There is a strong correlation between $\langle x \rangle$ and $\langle Q^2 \rangle$ that does not allow to explore x and Q^2 dependence of the TMDs separetely. We notice that the agreement tends to improve as we move to higher Q^2 values, where the kinematic approximations of factorization are more reliable. Moreover, for fixed P_{hT} and Q^2, the agreement is in general better at higher z values, which also resembles the kinematic condition $P_{hT}/z \lesssim Q$ for TMD factorization.

Fig. 2 has same content and notation as in Fig. 1 but for kaons in the final state. Here we notice that the agreement at low z tends to be better than in the previous case of pion production.

In Fig. 3 we present COMPASS normalized multiplicities (see (36)) for production of π^- off a deuteron for different $\langle x \rangle$, $\langle z \rangle$, and $\langle Q^2 \rangle$ bins as a funciton of the transverse momentum of the dected hadron P_{hT}. The circle around the first P_{hT} point in each panel indicates that the first value is fixed and not fitted. The correlation between x and Q^2 is less strong than at HERMES and this allows to study different $\langle x \rangle$ bins at fixed $\langle Q^2 \rangle$. For the highest Q^2 the agreement is good for all $\langle x \rangle$, $\langle z \rangle$ and P_{hT}^2. In bins at lower Q^2, the descriptions is degraded and gets worse especially as z increases, contrary to HERMES data. For fixed $\langle Q^2 \rangle$ and high $\langle z \rangle$, a good agreement is recovered moving to higher $\langle x \rangle$ bins.

Fig. 4 has same content and notation as in Fig. 3 and the same comments on the agreement between theory and the data apply.

Drell-Yan processes

The low energy Drell-Yan data collected by the E288 and E605 experiments at Fermilab have large error bands (see Fig. 5). This is why the χ^2 values in Tab. VIII are rather low compared to the other data sets.

The agreement is also good for Z boson production, see Tab. IX. The statistics from Run-II is higher, which generates smaller experimental uncertainties and higher χ^2, especially for the CDF experiment.
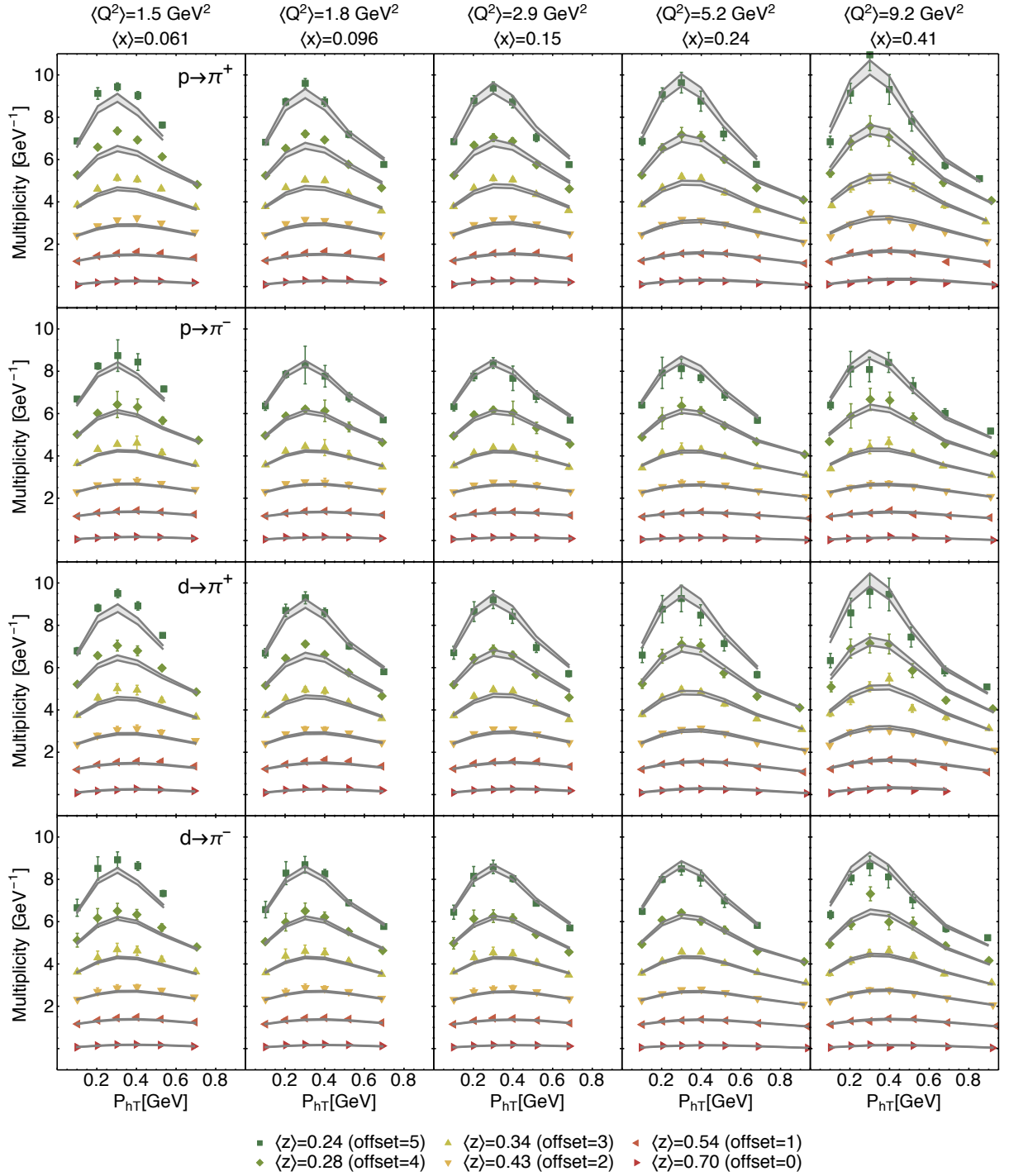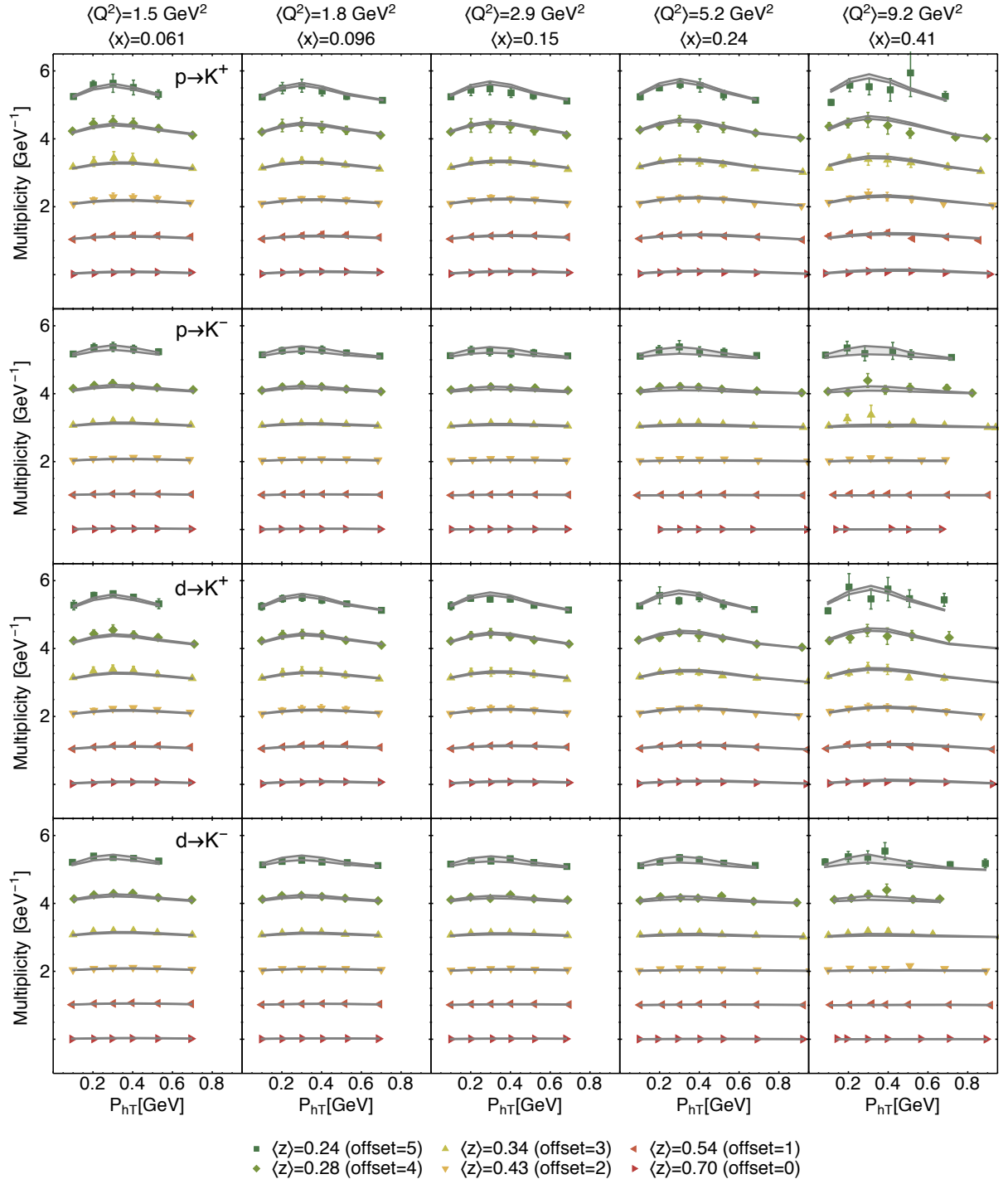
FIG. 1: Hermes multiplicities for production of pions off a proton and a deuteron for different $\langle x \rangle$, $\langle z \rangle$, and $\langle Q^2 \rangle$ bins as a funciton of the transverse momentum of the dected hadron P_{hT}.

Fig. 5 displays the cross section for DY events differential with respect to the transverse momentum q_T of the virtual photon, its invariant mass Q^2 and rapidity y. As for the case of SIDIS, the grey bands are the 68% C.L. envelope of the 200 replicas of the fit function. The four panels represents different values for the rapidity y or x_F (see (14)). In each panel, we have plots for different Q^2 values. The lower is Q, the less points in q_T we fit (see also
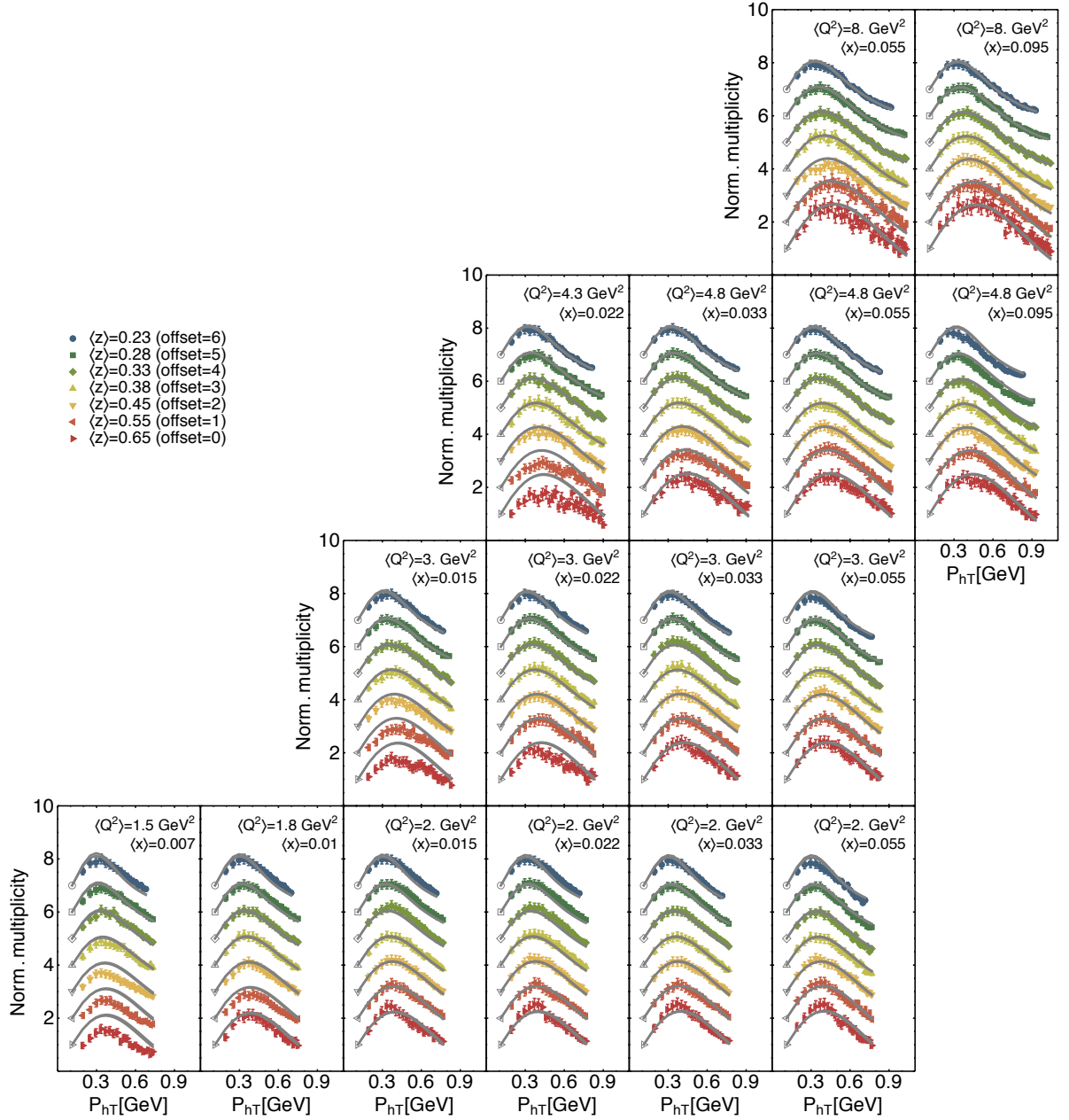
FIG. 2: Hermes multiplicities for production of kaons off a proton and a deuteron for different $\langle x \rangle$, $\langle z \rangle$, and $\langle Q^2 \rangle$ bins as a funciton of the transverse momentum of the dected hadron P_{hT}.

Sec. III C). The hard scale lies in the region $4.5 < \langle Q \rangle < 13.5$ GeV. This region is of particular importance, since these "moderate" Q values are high enough to safely apply factorization without pollution from higher twist effects and from the very low b_T region and, at the same time, low enough in order for the nonperturbative effects to not be shaded by transverse momentum resummation. A visible effect of TMD evolution is the shift of the peak position to

FIG. 3: Compass multiplicities for production of negative hadrons (π^-) off a deuteron for different $\langle x \rangle$, $\langle z \rangle$, and $\langle Q^2 \rangle$ bins as a funciton of the transverse momentum of the dected hadron P_{hT}. Multiplicities are normalized to the first bin in P_{hT} for each $\langle z \rangle$ value (see (36)). For clarity, each $\langle z \rangle$ bin has been shifted by an offset indicated in the legend.

higher q_T as Q increases (effect visible in each panel in Fig. 5). In Fig. 6 we compare the cross section differential with respect to the transverse momentum q_T of the virtual Z (namely Eq. (11) integrated over η) with data from CDF and D0 at Tevatron Run I and II. Due to the higher $Q = M_Z$, the range explored in q_T is much larger compared to all the other observables considered. The tails of the distributions clearly deviate from a Gaussian behavior, as it is also evident in the bins at higher Q^2 in Fig. 5. The band from the replica methodology in this case is much narrower, due
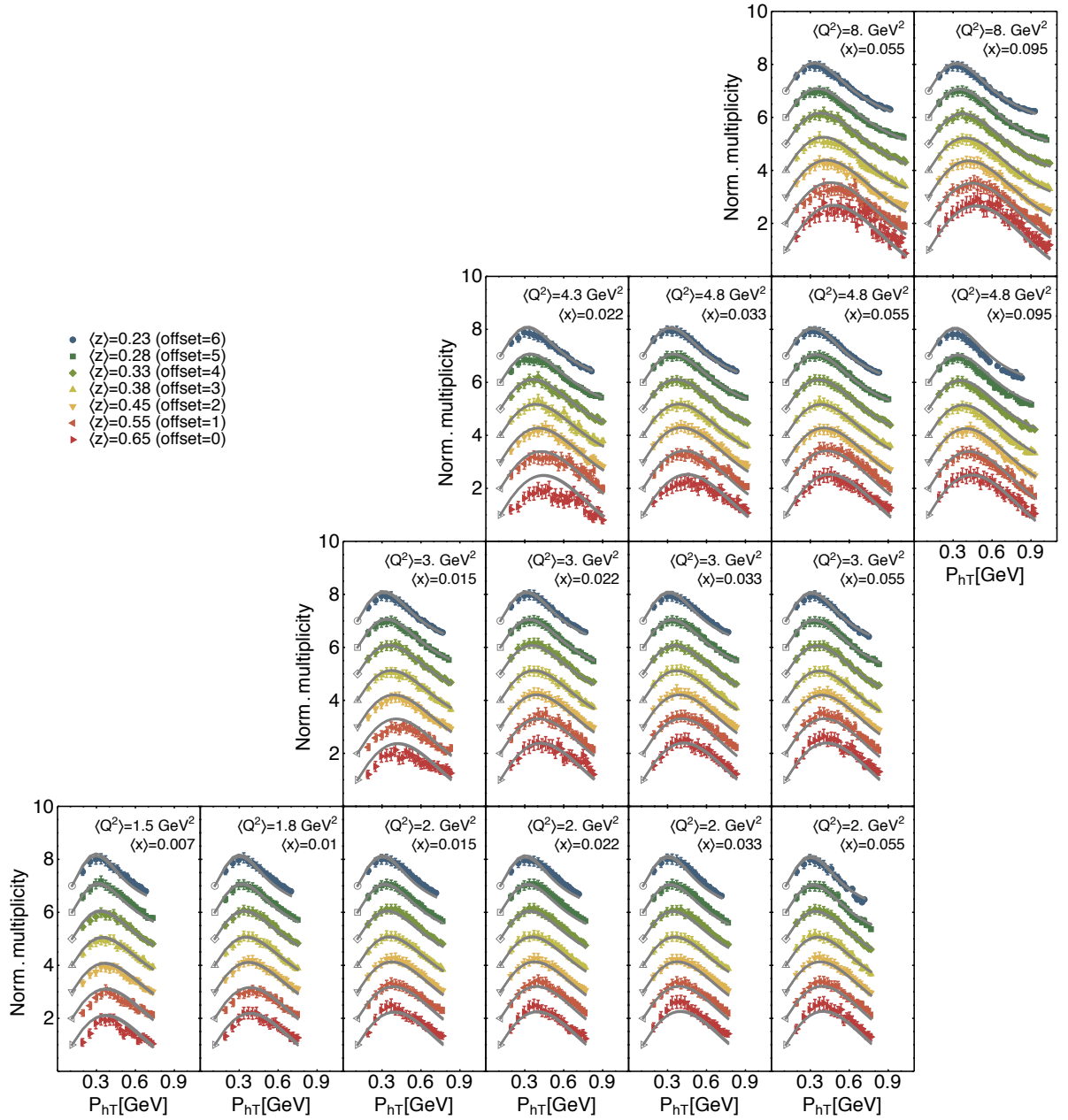
FIG. 4: Compass multiplicities for production of positive hadrons (π^{+}) off a deuteron for different $\langle x \rangle$, $\langle z \rangle$, and $\langle Q^2 \rangle$ bins as a funciton of the transverse momentum of the dected hadron P_{hT}. Multiplicities are normalized to the first bin in P_{hT} for each $\langle z \rangle$ value (see (36)). For clarity, each $\langle z \rangle$ bin has been shifted by an offset indicated in the legend.

to the reduced sensitivity to the intrinsic transverse momenta at $Q = M_Z$ and to the limited range of best-fit values for the parameter g_2, which controls soft-gluon emission. As an effect of TMD evolution, the peak shifts from ~ 1 GeV for Drell-Yan events in Fig. 5 to ~ 5 GeV in Fig. 6. The position of the peak is affected both by the perturbative and the nonperturbative part of the Sudakov exponent (see Sec. II C and [21]). Most of the contributions to the χ^2 comes from normalization effects and not from the shape in q_T.

	E288 [200]	E288 [300]	E288 [400]	E605
Points	45	45	78	35
χ^2/points	0.99	0.84	0.32	1.12

TABLE VIII: Number of points analyzed and χ^2 values for fixed-target Drell-Yan experiments at low energy. The labels in square brackets were introduced in Sec. III C.

	CDF Run I	D0 Run I	CDF Run II	D0 Run II
Points	31	14	37	8
χ^2/points	1.36	1.11	2.00	1.73

TABLE IX: Number of points analyzed and χ^2 values for Z boson production at Tevatron.
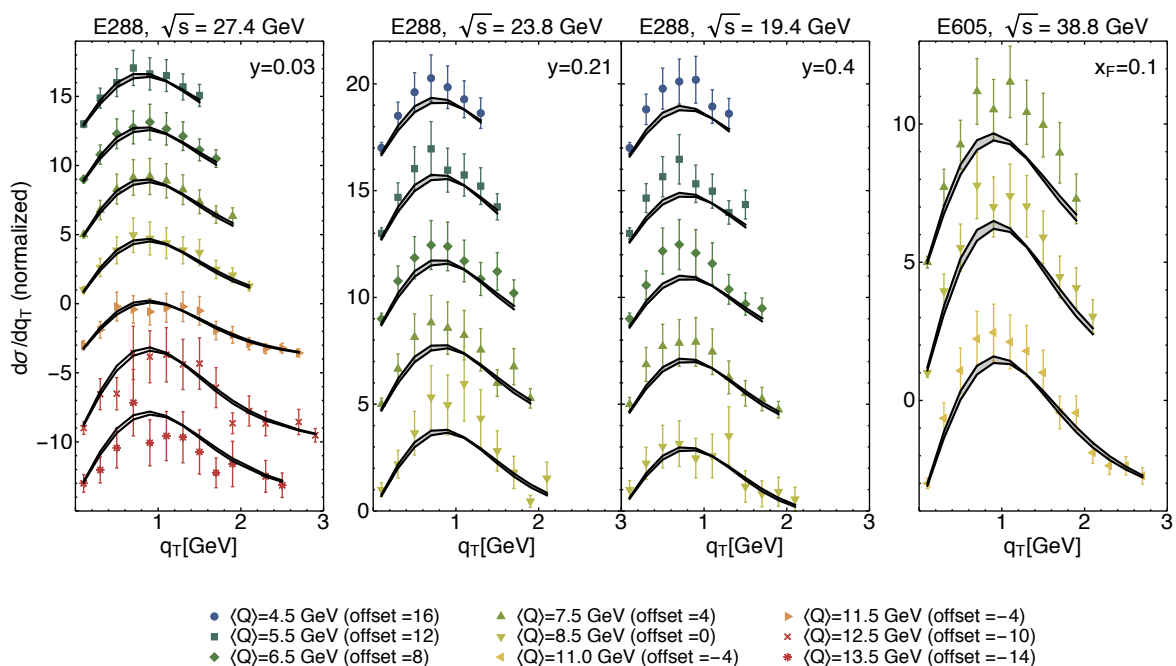
FIG. 5: Drell-Yan differential cross section for different experiments and different values of $\sqrt{s}$ and for different $\langle Q \rangle$ bins. For clarity, each $\langle Q \rangle$ bin has been shifted by an offset indicated in the legend. AS: is the cross section differential in Q^2 and rapidity η (or y?) "Normalized"=?

B. Transverse momentum dependence at 1 GeV

The variables $b_{\min}$ and $b_{\max}$ delimit the range in b_T where transverse momentum resummation is computed perturbatively. $b_{\max}$ allows to avoid the Landau pole and $b_{\min}$ allows to recover correctly the high transverse momentum limit of the cross section (see also Sec. II C). The parameter g_2 which enters the nonperturbative Sudakov exponent quantifies the amount of soft gluons radiated. As already detailed in Sec. II C, in this work we fix the value for $b_{\min}$ and $b_{\max}$ in such a way that at $Q = 1$ GeV the unpolarized TMDs coincide with their nonperturbative input. g_2, instead, is a fit parameter.

Tab. X summarizes the chosen values of $b_{\min}$, $b_{\max}$ and the best-fit value for g_2. The latter is given as an average with 68% C.L. uncertainty computed over the set of 200 replicas. A similar value ($g_2 = 0.184 \pm 0.018$) was found in [43]. We stress here that a prescription involving both $b_{\min}$ and $b_{\max}$ is equivalent to request $\mu_{b^*}^2 < Q^2 \equiv \mu^2$ for
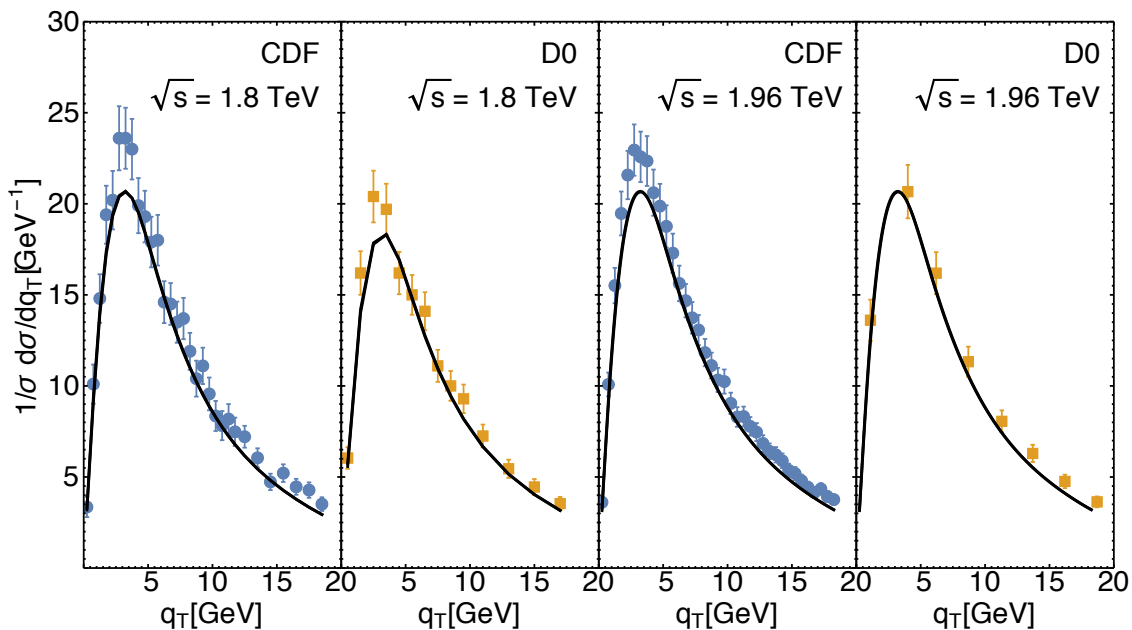
FIG. 6: Cross section differential with respect to the transverse momentum q_T of a Z boson produced from $p\bar{p}$ collisions at Tevatron. The four panels refer to different experiments (CDF and D0) with two different values for the center-of-mass energy ($\sqrt{s} = 1.8$ TeV and $\sqrt{s} = 1.96$ TeV). In this case the band is narrow due to the narrow range for the best-fit values of g_2.

all b_T values in (26). This requirement turns out to be crucial in order to fit SIDIS data with TMD evolution and without a Y-term.

Tab. XI collects the best-fit values of parameters in the nonperturbative part of the TMDs at $Q = 1$ GeV (see (30) and (31)); we give the average value over the full set of replicas and the standard deviation based on a 68% C.L. (see Sec. III E). We also compare these values with the best-values from replica 105.

Keeping in mind that $\langle \hat{\boldsymbol{k}}_\perp^2 \rangle = \langle \boldsymbol{k}_\perp^2 \rangle (x = 0.1)$ and $\langle \hat{\boldsymbol{P}}_\perp^2 \rangle = \langle \boldsymbol{P}_\perp^2 \rangle (z = 0.5)$, we note that the average value of $\langle \hat{\boldsymbol{k}}_\perp^2 \rangle$ is similar to and compatible within error bands with the value given in [22] for the flavor-independent scenario. The value of $\langle \hat{\boldsymbol{P}}_\perp^2 \rangle$ is larger but still compatible with the same quantity given in [22]. Comparisons between the two fits are anyway delicate, since here we rely on a modified Gaussian ansatz, see (32) and (33). Fig. 7 is useful to compare diffferent extractions of partonic transverse momenta. The red area corresponds to the 68% confidence region for $\{\langle \hat{\boldsymbol{k}}_\perp^2 \rangle, \langle \hat{\boldsymbol{P}}_\perp^2 \rangle\}$ pairs. Each black dot is an outcome of one fit (replica). The same applies to the orange region and its black dots, related to the flavor-independent analysis in [22]. All the other points are related to different extractions and the color coding is described in the caption of Fig. 7. From the orange region (fit of SIDIS at HERMES only) a strong anticorrelation between the transverse momenta is evident. The inclusion of Drell-Yan and Z production data adds physical information about the nonperturbative structure of $f_1(x, k_\perp^2)$. This significantly reduces the spread in $\langle \hat{\boldsymbol{k}}_\perp^2 \rangle$ and the correlation with $\langle \hat{\boldsymbol{P}}_\perp^2 \rangle$ (see the red region). The inclusion of COMPASS data, instead, determines a shift of the points and reduces the spread for $\langle \hat{\boldsymbol{P}}_\perp^2 \rangle$ values. These are important features of the fit and we should aim at including e^+e^- data too to further reduce the correlation. Ideally in a global fit we will reach the lowest degree of correlation possible. When comparing different extractions, it is important to keep in mind that the intrinsic transverse momentum always depends on the scheme used to implement TMD evolution and its accuracy.

Tab. XI also presents the best-fit values for parameters shaping the kinematic dependence of $\langle \boldsymbol{k}_\perp^2 \rangle (x)$, $\langle \boldsymbol{P}_\perp^2 \rangle (z)$, $\langle \boldsymbol{P}\perp'^2 \rangle (z)$ (see (34) and (35)). Since the values are all positive the average square transverse momenta cannot diverge in the limits $x, z \to 0$ or 1. The kinematic dependence is shown in Fig. 8 (a) for $\langle \boldsymbol{k}_\perp^2 \rangle (x)$ and Fig. 8 (b) for $\langle \boldsymbol{P}_\perp^2 \rangle (z)$. The plot for $\langle \boldsymbol{P}\perp'^2 \rangle (z)$ is identical to Fig. 8 (b) apart from a normalization factor. The pink bands are computed

as the 68% C.L. envelope of the full sets of curves from the 200 replicas. Comparison with other extractions are presented and the legenda is detailed in the caption of Fig. 7.

AS: shall we add plots for $f_1(x, k_\perp^2)$ and $D_1(z, P_\perp^2)$ to illustrate their shape at $Q = 1$ GeV in momentum space?

	b_{max} [GeV^{-1}] (fixed)	b_{min} [GeV^{-1}] (fixed)	g_2 [GeV^2]
All replicas	$2e^{-\gamma_E}$ [/GeV]	$2e^{-\gamma_E}/Q$	0.13 ± 0.01
Replica 105	$2e^{-\gamma_E}$ [/GeV]	$2e^{-\gamma_E}/Q$	0.128

TABLE X: Values of parameters common to TMD PDFs and TMD FFs.

TMD PDFs	$\langle \hat{\boldsymbol{k}}_\perp^2 \rangle$ [GeV^2]	α	σ		λ [GeV^{-2}]	
All replicas	0.28 ± 0.06	2.95 ± 0.05	0.17 ± 0.02		0.86 ± 0.78	
Replica 105	0.285	2.98	0.173		0.39	
TMD FFs	$\langle \hat{\boldsymbol{P}}_\perp^2 \rangle$ [GeV^2]	β	δ	γ	λ_F [GeV^{-2}]	$\langle \hat{\boldsymbol{P}}_\perp'^2 \rangle$ [GeV^2]
All replicas	0.21 ± 0.02	1.65 ± 0.49	2.28 ± 0.46	0.14 ± 0.07	5.50 ± 1.23	0.13 ± 0.01
Replica 105	0.212	2.10	2.52	0.094	5.29	0.135

TABLE XI: 68% confidence intervals of best-fit values for parametrizations of TMDs at $Q = 1$ GeV.
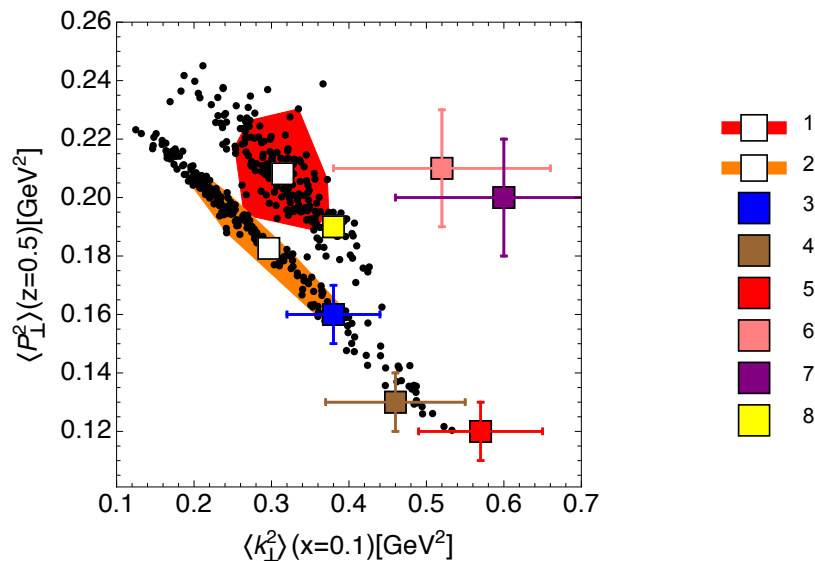

FIG. 7: Correlation between transverse momenta in TMD FFs, $\langle P_\perp^2 \rangle (z = 0.5)$, and in TMD PDFs, $\langle k_\perp^2 \rangle (x = 0.1)$, in different phenomenological extractions. The red region is the 68% C.L. area explored in this fit (1-red). The white boxes represent the average values over the replicas for the transverse momenta. The other extractions are: (2-orange) [22], (3-blue) [65], (4-brown) [48] for HERMES data, (5-red point) [48] for HERMES data at high z, (6-pink) [48] for normalized COMPASS data, (7-purple) [48] for normalized COMPASS data at high z, (8-yellow) [15]. For more details, such as the value of the input scale for the TMDs, see the respective references.
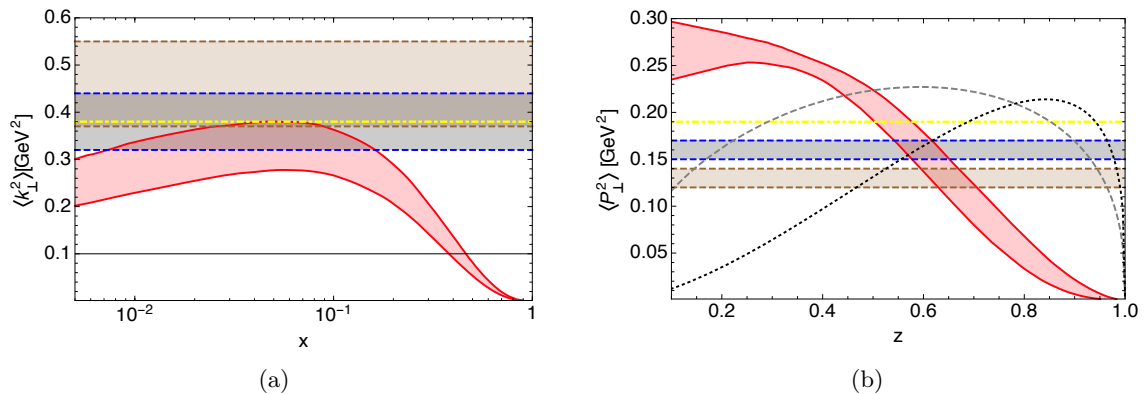
(a)   (b)

FIG. 8: Kinematic dependence of $\langle \boldsymbol{k}_\perp^2 \rangle (x)$ (a) and of $\langle \boldsymbol{P}_\perp^2 \rangle (z)$ (b). The bands are the 68% C.L. envelope of the full sets of best-fit curves. Comparisons with other extractions are displayed. Color coding is the same as in Fig. 7. In (b) the grey-dashed curve refers to the parametrization used in GMCtrans [66] and the black-dashed curve refers to [67].

C. Tests on replica 105

In this subsection we have a closer look at the results of the fit to replica 105, which, as discussed above, is one of the most representative of the two hundred fits performed in our analysis. The corresponding $\chi^2/\text{d.o.f.}$ is 1.51. We note that if we normalize HERMES data to the value of the first bin in P_{hT} as we did for COMPASS data, the global $\chi^2/\text{d.o.f.}$ immediately reduces to 1.27, without performing any new minimization. The partial χ^2 for the different SIDIS processes measured at HERMES are shown in Table XII.

	$p \to \pi^+$	$p \to \pi^-$	$p \to K^+$	$p \to K^-$	$D \to \pi^+$	$D \to \pi^-$	$D \to K^+$	$D \to K^-$
Original	5.18	2.67	0.75	0.78	3.63	2.31	1.12	2.27
Normalized	1.94	1.13	0.57	0.29	1.59	0.80	0.47	0.97

TABLE XII: $\chi^2/\text{d.o.f.}$ for HERMES data with and without normalization to the value of the first bin in P_{hT}.

If we consider more stringent kinematic cuts on SIDIS data, namely $Q^2 > 1.5$ GeV^2 and $0.25 < z < 0.6$ instead of $Q^2 > 1.4$ GeV^2 and $0.2 < z < 0.7$, leaving the other ones unchanged, the number of bins reduces from 8059 to 5679. As a consequence, the $\chi^2/\text{d.o.f.}$ decreases to the value 1.23. In addition, if we replace the constraint $P_{hT} < \text{Min}[0.2\,Q, 0.7\,Qz] + 0.5$ with $P_{hT} < \text{Min}[0.2\,Q, 0.5\,Qz] + 0.3$, the number of bins becomes 3380 and the $\chi^2/\text{d.o.f.}$ decreases further to 0.96. By adopting the cut $P_{hT} < \text{Min}[0.2\,Q, 0.2\,Qz]$ instead, the number of bins drops to 477, with a $\chi^2/\text{d.o.f.} = 1.02$.

Finally, we consider the sensitivity of our results on the set of parameterizations adopted for the collinear, unpolarized quark distributions. The $\chi^2/\text{d.o.f.}$ varies from its original value 1.51, obtained with the NLO GJR 2008 parametrization [?], to 1.84 (NLO MSTW 2008 [?]) and 1.85 (NLO CJ12 [?]).

D. Comments on flavor-dependent fits

AS: do we want to comment on the difficulties encountered while fitting with a flavor-dependent scheme for the transverse momentum dependence? In my opinion we should do it, but I also think that we should aim at conveying a positive message. For example, we could talk about some of the tests that we have performed excluding COMPASS data.

V. SUMMARY AND OUTLOOK

In this work we demonstrated for the first time the possibility to perform a rigorous simultaneous fit of unpolarized TMDs to data of SIDIS, Drell-Yan, and Z boson production collected by different experiments. This constitutes the

first attempt towards a global fitting strategy for $f_1^a(x, k_\perp^2)$ and $D_1^{a \to h}(z, P_\perp^2)$ in the context of TMD factorization. We plan to release grids of the parametrizations studied in this work via TMDlib [68] to facilitate phenomenological studies for present and future experiments.

We extracted unpolarized TMDs using 8059 data points with 11 free parameters using a replica methodology. We choose $Q^2 > 1.4$ GeV^2, $0.2 < z < 0.7$ and phenomenological implementations of the small transverse momentum region (see Sec. III). The average χ^2/d.o.f. is 1.55 ± 0.05. Most of the discrepancies between experimental data and theory comes from the normalisation and not from the shape in transverse momentum. This might indicate the both perturbative corrections and higher-twist corrections could play a relevant role at low energies.

This fit is performed assuming that the intrinsic transverse momentum dependence is described by a normalized linear combination of a Gaussian and a weigthed Gaussian in momentum space. For f_1 we assume that the two Gaussian distributions have the same variance, for D_1 we relax this condition. To describe the high transverse momentum tail of the TMDs, we include TMD evolution at NLL in the Sudakov exponenet and at LO in the Wilson coefficients matching onto collinear distributions.

By means of fitting data from different processes and experiments, we also perform a phenomenological check of the universality of unpolarized TMDs. TMD factorization allows us to describe the considered data in a reasonable way at low transverse momentum. In future works we should aim at a more precise analysis from the perturbative point of view, at a detailed flavor decomposition in momentum space and at describing also events at higher transverse momenta matching to the collinear fixed-order calculations. We look also forward to the possibility of identifying the current fragmentation region in a more sistematic way [34]. Together with an improved theoretical framework, in order to better understand the formalism we need more experimental data. In particular with larger coverage in x, z and rapidity and spanning over a larger range in Q^2. Additional data from SIDIS (at Jefferson Lab, at a future Electron-Ion Collider), Drell-Yan, Z/W production (at COMPASS , at the LHC, at RHIC, at A Fixed-Target Experiment at the LHC) and e^+e^- (at Belle-II, BES-III, at a future Internation Linear Collider) will be very important.

Testing the formalism of TMD factorization and understanding the structure of unpolarized TMDs is only the first crucial step in the exploration of the 3D proton structure in momentum space and this work opens the way to global determinations of TMDs. Building on this, we can proceed to deepen our understanding of hadron structure via asymmetries and polarized structure function (see e.g. [69–71]) and, at the same time, to test the impact of hadron structure in precision measurements at high-energies, such as at the LHC. A detailed mapping of hadron structure is essential to interpret data from hadronic collisions, which are among the most powerful tools to look for footprints of new physics. In particular, the 12 GeV physics program at Jefferson Lab [72] will be very important to constrain collinear and TMD distributions at large x, fundamental in order to search new heavy particles at hadron colliders.

[1] J. C. Collins, D. E. Soper, and G. Sterman, Adv. Ser. Direct. High Energy Phys. **5**, 1 (1989), hep-ph/0409313.
[2] J. Collins, *Foundations of Perturbative QCD*, Cambridge Monographs on Particle Physics, Nuclear Physics and Cosmology (Cambridge University Press, 2011), ISBN 9780521855334, URL http://books.google.it/books?id=0xGi1KW9vykC.
[3] R. Angeles-Martinez et al., Acta Phys. Polon. **B46**, 2501 (2015), 1507.05267.
[4] T. C. Rogers, Eur. Phys. J. **A52**, 153 (2016), 1509.04766.
[5] A. Bacchetta, Eur. Phys. J. **A52**, 163 (2016).
[6] M. Radici, AIP Conf. Proc. **1735**, 020003 (2016).
[7] P. J. Mulders and R. D. Tangerman, Nucl. Phys. **B461**, 197 (1996), erratum-ibid. **B484** (1997) 538, hep-ph/9510301.
[8] A. Bacchetta, M. Diehl, K. Goeke, A. Metz, P. J. Mulders, and M. Schlegel, JHEP **02**, 093 (2007), hep-ph/0611265.
[9] D. Boer and P. J. Mulders, Phys. Rev. **D57**, 5780 (1998), hep-ph/9711485.
[10] A. Bacchetta and P. J. Mulders, Phys. Rev. **D62**, 114004 (2000), hep-ph/0007120.
[11] P. J. Mulders and J. Rodrigues, Phys. Rev. **D63**, 094021 (2001), hep-ph/0009343.
[12] D. Boer, S. Cotogno, T. van Daal, P. J. Mulders, A. Signori, and Y.-J. Zhou, JHEP **10**, 013 (2016), 1607.01654.
[13] A. Bacchetta and M. Radici, Phys.Rev.Lett. **107**, 212001 (2011), 1107.5755.

[14] M. Anselmino, M. Boglione, and S. Melis, Phys.Rev. **D86**, 014028 (2012), 1204.1239.
[15] M. G. Echevarria, A. Idilbi, Z.-B. Kang, and I. Vitev, Phys. Rev. **D89**, 074013 (2014), 1401.5078.
[16] Z. Lu and I. Schmidt, Phys. Rev. **D81**, 034023 (2010), 0912.2031.
[17] V. Barone, M. Boglione, J. O. Gonzalez Hernandez, and S. Melis, Phys. Rev. **D91**, 074019 (2015), 1502.04214.
[18] C. Lefky and A. Prokudin, Phys. Rev. **D91**, 034010 (2015), 1411.0580.
[19] M. Anselmino, M. Boglione, U. D'Alesio, S. Melis, F. Murgia, et al., Phys.Rev. **D87**, 094019 (2013), 1303.3822.
[20] Z.-B. Kang, A. Prokudin, P. Sun, and F. Yuan, Phys. Rev. **D93**, 014009 (2016), 1505.05589.
[21] A. Signori, Ph.D. thesis, Vrije U., Amsterdam (2016), URL http://inspirehep.net/record/1493030/files/Thesis-2016-Signori.pdf.
[22] A. Signori, A. Bacchetta, M. Radici, and G. Schnell, JHEP **1311**, 194 (2013), 1309.3507.
[23] A. Bacchetta, M. G. Echevarria, P. J. G. Mulders, M. Radici, and A. Signori, JHEP **11**, 076 (2015), 1508.00402.
[24] J. Collins, L. Gamberg, A. Prokudin, T. C. Rogers, N. Sato, and B. Wang, Phys. Rev. **D94**, 034014 (2016), 1605.00671.
[25] A. Bacchetta, D. Boer, M. Diehl, and P. J. Mulders, JHEP **08**, 023 (2008), 0803.0227.
[26] J. C. Collins and D. E. Soper, Nucl. Phys. **B193**, 381 (1981).
[27] J. C. Collins, D. E. Soper, and G. Sterman, Nucl. Phys. **B250**, 199 (1985).
[28] X. Ji and F. Yuan, Phys. Lett. **B543**, 66 (2002), hep-ph/0206057.
[29] X. Ji, J.-P. Ma, and F. Yuan, Phys. Rev. **D71**, 034005 (2005), hep-ph/0404183.
[30] S. Aybat and T. C. Rogers, Phys. Rev. **D83**, 114042 (2011), 1101.5057.
[31] M. G. Echevarria, A. Idilbi, and I. Scimemi, JHEP **1207**, 002 (2012), 1111.4996.
[32] M. G. Echevarri, A. Idilbi, A. Schfer, and I. Scimemi, Eur.Phys.J. **C73**, 2636 (2013), 1208.1281.
[33] J. C. Collins and T. C. Rogers, Phys.Rev. **D87**, 034018 (2013), 1210.2100.
[34] M. Boglione, J. Collins, L. Gamberg, J. O. Gonzalez-Hernandez, T. C. Rogers, and N. Sato, Phys. Lett. **B766**, 245 (2017), 1611.10329.
[35] D. Boer and W. Vogelsang, Phys. Rev. **D74**, 014004 (2006), hep-ph/0604177.
[36] S. Arnold, A. Metz, and M. Schlegel, Phys. Rev. **D79**, 034005 (2009), 0809.2262.
[37] E. Laenen, G. F. Sterman, and W. Vogelsang, Phys. Rev. Lett. **84**, 4296 (2000), hep-ph/0002078.
[38] G. Parisi and R. Petronzio, Nucl.Phys. **B154**, 427 (1979).
[39] G. Bozzi, S. Catani, G. Ferrera, D. de Florian, and M. Grazzini, Phys. Lett. **B696**, 207 (2011), 1007.2351.
[40] J. Collins and T. Rogers, Phys. Rev. **D91**, 074020 (2015), 1412.3820.
[41] P. M. Nadolsky, D. R. Stump, and C. P. Yuan, Phys. Rev. **D61**, 014003 (2000), hep-ph/9906280.
[42] F. Landry, R. Brock, P. M. Nadolsky, and C. P. Yuan, Phys. Rev. **D67**, 073016 (2003), hep-ph/0212159.
[43] A. V. Konychev and P. M. Nadolsky, Phys. Lett. **B633**, 710 (2006), hep-ph/0506225.
[44] C. A. Aidala, B. Field, L. P. Gamberg, and T. C. Rogers, Phys. Rev. **D89**, 094002 (2014), 1401.2654.
[45] U. D'Alesio, M. G. Echevarria, S. Melis, and I. Scimemi, JHEP **11**, 098 (2014), 1407.3311.
[46] A. Airapetian et al. (HERMES Collaboration), Phys. Rev. **D87**, 074029 (2013), 1212.5407.
[47] C. Adolph et al. (COMPASS), Eur. Phys. J. **C73**, 2531 (2013), [Erratum: Eur. Phys. J.C75,no.2,94(2015)], 1305.7317.
[48] M. Anselmino, M. Boglione, J. O. G. H., S. Melis, and A. Prokudin (2013), 1312.6261.
[49] U. D'Alesio, M. G. Echevarria, S. Melis, and I. Scimemi, JHEP **11**, 098 (2014), 1407.3311.
[50] A. S. Ito et al., Phys. Rev. **D23**, 604 (1981).
[51] G. Moreno et al., Phys. Rev. **D43**, 2815 (1991).
[52] T. Affolder et al. (CDF), Phys. Rev. Lett. **84**, 845 (2000), hep-ex/0001021.
[53] B. Abbott et al. (D0), Phys. Rev. **D61**, 032004 (2000), hep-ex/9907009.
[54] T. Aaltonen et al. (CDF), Phys. Rev. **D86**, 052010 (2012), 1207.7138.
[55] V. M. Abazov et al. (D0), Phys. Rev. Lett. **100**, 102002 (2008), 0712.0803.
[56] A. Bacchetta, A. Courtoy, and M. Radici, JHEP **1303**, 119 (2013), 1212.3568.
[57] M. Radici, A. Courtoy, A. Bacchetta, and M. Guagnelli, JHEP **05**, 123 (2015), 1503.03495.
[58] S. Forte, L. Garrido, J. I. Latorre, and A. Piccione, JHEP **0205**, 062 (2002), hep-ph/0204232.
[59] R. D. Ball et al. (NNPDF Collaboration), Nucl. Phys. **B809**, 1 (2009), 0808.1231.
[60] R. D. Ball et al., Nucl. Phys. **B838**, 136 (2010), 1002.4407.
[61] D. de Florian, R. Sassot, M. Epele, R. J. Hernndez-Pinto, and M. Stratmann, Phys. Rev. **D91**, 014035 (2015), 1410.6027.
[62] D. de Florian, R. Sassot, and M. Stratmann, Phys. Rev. **D75**, 114010 (2007), hep-ph/0703242.
[63] M. Epele, R. Llubaroff, R. Sassot, and M. Stratmann, Phys. Rev. **D86**, 074028 (2012), 1209.3240.
[64] A. Signori, A. Bacchetta, and M. Radici, Int. J. Mod. Phys. Conf. Ser. **25**, 1460020 (2014), 1309.5929.
[65] P. Schweitzer, T. Teckentrup, and A. Metz, Phys. Rev. **D81**, 094019 (2010), 1003.2190.
[66] A. Bacchetta, U. Elschenbroich, Y. Miyachi, G. Schnell, T. Shibata, Y. Takubo, H. Tanaka, and R. Seidl, HERMES Internal Report 04-039 (2004).
[67] M. Boglione and P. J. Mulders, Phys. Rev. **D60**, 054007 (1999), hep-ph/9903354.
[68] F. Hautmann, H. Jung, M. Krmer, P. J. Mulders, E. R. Nocera, T. C. Rogers, and A. Signori, Eur. Phys. J. **C74**, 3220 (2014), 1408.3015.
[69] E. C. Aschenauer, U. D'Alesio, and F. Murgia, Eur. Phys. J. **A52**, 156 (2016), 1512.05379.
[70] M. Boglione and A. Prokudin, Eur. Phys. J. **A52**, 154 (2016), 1511.06924.
[71] D. Kiko?a, M. G. Echevarria, C. Hadjidakis, J.-P. Lansberg, C. Lorc, L. Massacrier, C. M. Quintans, A. Signori, and B. Trzeciak (2017), 1702.01546.
[72] J. Dudek, R. Ent, R. Essig, K. Kumar, C. Meyer, et al., Eur.Phys.J. **A48**, 187 (2012), 1208.1244.